Quantum electrodynamical theory of high-efficiency excitation energy transfer in laser-driven nanostructure systems

Dilusha Weeraddana[*] and Malin Premaratne[†]
Advanced Computing and Simulation Laboratory (AχL), Department of Electrical and Computer Systems Engineering, Monash University, Clayton, Victoria 3800, Australia

Sarath D. Gunapala[‡]
Jet Propulsion Laboratory, California Institute of Technology, Pasadena, California 91109, USA

David L. Andrews[§]
School of Chemistry, University of East Anglia, Norwich Research Park, Norwich NR4 7TJ, United Kingdom
(Received 17 May 2016; published 17 August 2016)

A fundamental theory is developed for describing laser-driven resonance energy transfer (RET) in dimensionally constrained nanostructures within the framework of quantum electrodynamics. The process of RET communicates electronic excitation between suitably disposed emitter and detector particles in close proximity, activated by the initial excitation of the emitter. Here, we demonstrate that the transfer rate can be significantly increased by propagation of an auxiliary laser beam through a pair of nanostructure particles. This is due to the higher order perturbative contribution to the Förster-type RET, in which laser field is applied to stimulate the energy transfer process. We construct a detailed picture of how excitation energy transfer is affected by an off-resonant radiation field, which includes the derivation of second and fourth order quantum amplitudes. The analysis delivers detailed results for the dependence of the transfer rates on orientational, distance, and laser intensity factor, providing a comprehensive fundamental understanding of laser-driven RET in nanostructures. The results of the derivations demonstrate that the geometry of the system exercises considerable control over the laser-assisted RET mechanism. Thus, under favorable conformational conditions and relative spacing of donor-acceptor nanostructures, the effect of the auxiliary laser beam is shown to produce up to 70% enhancement in the energy migration rate. This degree of control allows optical switching applications to be identified.

DOI: 10.1103/PhysRevB.94.085133

I. INTRODUCTION

In many of the most promising advances in photonics, the development of semiconductor nanowires and quantum dot materials is leading to numerous next-generation applications [1–4]. The quantum confinement in these materials makes them capable of providing unique and superior optical properties. Thus, nanowires and quantum dots are becoming increasingly prominent at the very heart of modern nanophotonics [5–9]. In particular, exciton-exciton interactions through nonradiative resonance energy transfer (RET) of these dimensionally constrained nanostructures have enabled exciting opportunities to be identified in light generation and energy harvesting [10–12].

RET is a mechanism that exerts significant control across a chemically diverse and extensive range of material systems [13–18]. In nature, energy from the sunlight is captured by photobiological antenna chromophores, and subsequently transferred to a reaction center by a series of hops between other chromophore units with great efficiency by RET [19,20]. The phenomenon also has an important function in the operation of organic light-emitting diodes, solar light harvesting, and luminescence detectors [13,21,22].

The process of resonance energy transfer was first correctly described by Förster [23], and is also known as Förster resonance energy transfer (FRET). FRET can be described as the transfer of the excitation energy from an excited donor to a ground-state detector without the process of real photon emission/reabsorption. This mechanism of transfer of energy in the near field occurs due to the Coulombic interaction between the resonant transition dipoles of donor and detector species. Furthermore, RET was first discussed in terms of quantum electrodynamics (QED) in pioneering studies by Avery [24] and Gomberoff and Power [25]. These studies showed that far-field retardation effects embellish a near-field Coulombic interaction and, radiative and radiationless mechanisms are both necessarily incorporated within a common theory as asymptotic limits. In fact, RET is fully quantum mechanical in nature, and can be comprehensively analyzed considering a closed quantum mechanical system where both matter and radiation are quantized [26–29].

Moreover, it has been shown that electronically excited nanostructures interact with their neighbors differently from their ground-state counterparts [30,31]. It also emerges from the use of QED that a throughput off-resonant radiation can also produce significant additional effects on the process of RET between two molecules (laser-assisted resonance energy transfer) [32]. This is due to coupled absorption and stimulated emission of photons from and into the applied beam. Therefore, following conventional excitation of the donor particle, the transfer rate can be appreciably increased by the propagation of an auxiliary laser beam through the

[*]dilusha.weeraddana@monash.edu
[†]malin.premaratne@monash.edu
[‡]Sarath.D.Gunapala@jpl.nasa.gov
[§]d.l.andrews@uea.ac.uk

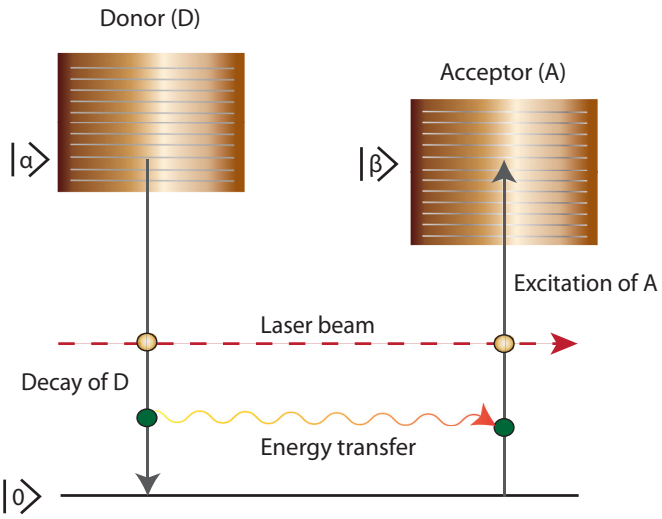

FIG. 1. Schematic depiction of energy transfer from donor to acceptor. Green arrows represent emission and absorption of energy in donor and acceptor particles. Horizontal red dashed arrow illustrates the interaction of the laser beam with the donor and acceptor. Horizontal orange wavy arrow represents the transfer of energy, mediated by a virtual photon, from the donor to the acceptor. The Greek letters indicate the relevant electronic excited states and 0 the ground state.

donor-acceptor system [33,34]. A schematic illustration of the laser-driven RET process is shown in Fig. 1.

However, the origin of the complications associated with laser-driven RET in nanostructures is deeply rooted in the nature of real and virtual photons which interact with confined geometries. Although the basic principles of RET are well established, there still exist open questions regarding the mechanisms of the RET phenomenon in many aspects.

Therefore, the main objective of this paper is to study the effects on the energy transfer process due directly to a laser field impinging on nanowire and quantum dot systems. We propose and model a system consisting of nanowires or quantum dots irradiated by an auxiliary laser beam, by developing a comprehensive quantum electrodynamical analysis. We show that the rate of resonance energy transfer can be greatly increased through an applied off-resonant radiation field under favorable physical configurations of nanostructures.

II. QED PERSPECTIVE OF LASER-ASSISTED RESONANCE ENERGY TRANSFER

We first review and sharpen the concept of RET based on the quantum theory of light-matter interaction. The key feature of quantum electrodynamics is that both the radiation and matter are subject to quantum mechanical rules. The system Hamiltonian comprises unperturbed operators for the two matter components, a source $H^D_{\rm mat}$ and detector $H^A_{\rm mat}$, two corresponding light-matter interaction terms, $H^D_{\rm int}$ and $H^A_{\rm int}$, and also the second-quantized radiation field $H_{\rm rad}$:

$$H_{\rm total} = H^D_{\rm mat} + H^A_{\rm mat} + H^D_{\rm int} + H^A_{\rm int} + H_{\rm rad}. \tag{1}$$

Here, in the superscripts distinguishing the source and detector, we retain the commonly used labels D and A (in other contexts signifying donor and acceptor). The eigenstates $|\tau\rangle$ of a basis Hamiltonian given in Eq. (1) form a composite set:

$$|\tau\rangle = |{\rm mat}_\tau\rangle|{\rm rad}_\tau\rangle \equiv |{\rm mat}_\tau; {\rm rad}_\tau\rangle. \tag{2}$$

Here, $|{\rm mat}_\tau\rangle$ defines the status of all nanostructures (or atoms, according to the system), comprising the vectors for each nanostructures particle (i.e., donor), and $|{\rm rad}_\tau\rangle$ is the radiation (number) states. Within the electric dipole approximation, the matter-field coupling Hamiltonian $H^\xi_{\rm int}$ ($\xi = D, A$) and $H_{\rm rad}$ are explicitly given by

$$H^\xi_{\rm int} = -\boldsymbol{\mu}(\xi)\cdot\boldsymbol{E}(\boldsymbol{R}_\xi), \tag{3}$$

$$H_{\rm rad} = \sum_{\mathbf{p},\lambda}\left[a^{\dagger(\lambda)}(\mathbf{p})a^{(\lambda)}(\mathbf{p})\hbar c p + \frac{1}{2}\right], \tag{4}$$

where the interaction Hamiltonian comprises contributions for each species ξ located at $\boldsymbol{R}_\xi$, the $\boldsymbol{\mu}(\xi)$ is the electric-dipole moment operator, and $\boldsymbol{E}(\boldsymbol{R}_\xi)$ is the operator for the electric displacement field at the specified location $\boldsymbol{R}_\xi$. The $\boldsymbol{\mu}(\xi)$ operates on matter states $|{\rm mat}_\tau\rangle$, and the $\boldsymbol{E}(\boldsymbol{R}_\xi)$ operates on $|{\rm rad}_\tau\rangle$. Moreover, in Eq. (4), the sum is taken over radiation modes characterized by wave vector $\mathbf{p}$ and polarization λ; $a^{\dagger(\lambda)}(\mathbf{p})$,$a^{(\lambda)}(\mathbf{p})$ are respectively the photon creation and annihilation operators for a mode ($\mathbf{p}$,λ), and p is the corresponding photon wave number.

The quantum probability amplitude or matrix element, M, is expressed through the time-dependent perturbation expansion:

$$M = \sum_{m=1}^{\infty} M^{(m)}, \tag{5}$$

where m is the number of photonic interactions. For the conventional direct energy transfer, leading contributions to the matrix element are associated with $m = 2$, expressive of the two interactions shown in Figs. 2(a) and 2(b) [26,34], and given by

$$M^{(2)} = \sum_R \frac{\langle F|H_{\rm int}|R\rangle\langle R|H_{\rm int}|I\rangle}{E_I - E_R}. \tag{6}$$

Here, to represent the energy transfer from donor to acceptor, the initial, final, and intermediate matter-radiation state vectors can be identified with corresponding eigenenergies with the energy identity [30]

$$E^D_{0\alpha} = E^A_{\beta 0} = \hbar c q, \tag{7}$$

where $\hbar c q$ is the physically identifiable transferred energy. This also represents the overall energy conservation identity.

The effects on the energy-transfer process manifest through interaction with an auxiliary beam; the lowest-order contribution to effect a rate modification will be due to two extra laser-particle interactions. As depicted in Figs. 2(c)–2(f), depending on how the throughput radiation interacts with the emitter-detector system, a number of possible laser-modified energy transfer mechanisms emerge. Each entails real photon absorption and emission, coupled by a virtual photon mediator. Therefore, the quantum amplitude which accounts for these corrections is a fourth-order perturbational theory summing

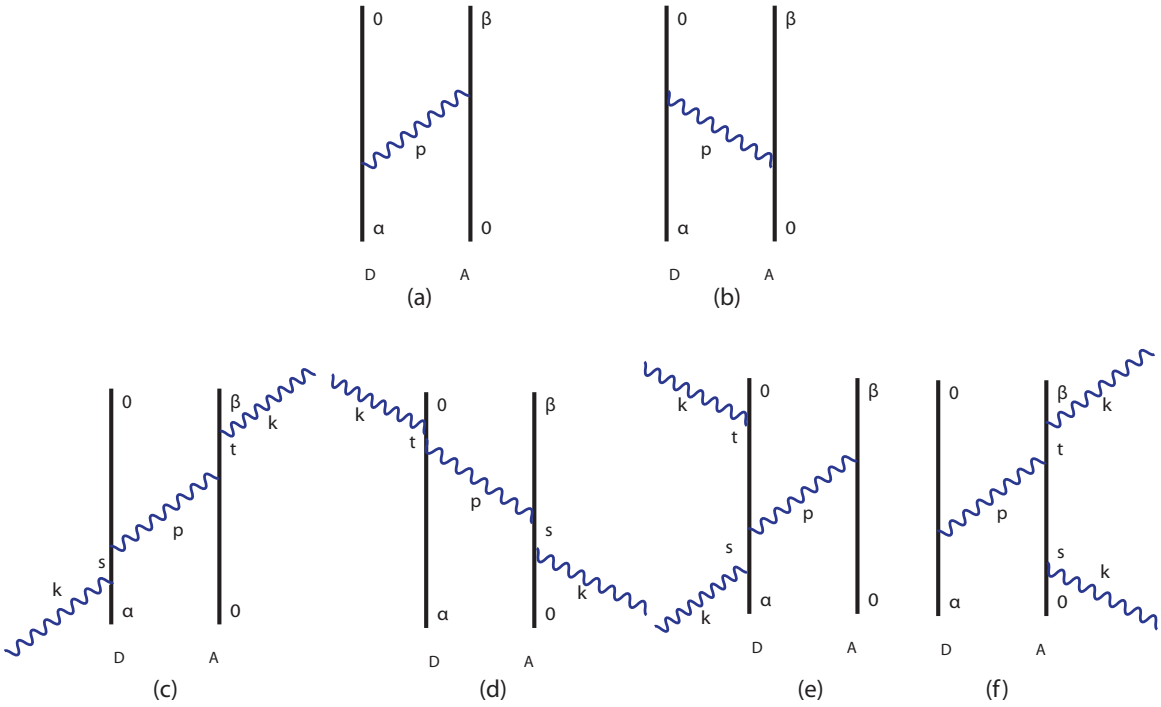

FIG. 2. Time-ordered Feynman diagrams representing resonance energy transfer between a donor D and acceptor A. On each matter vertical line, Greek symbols identify particle electronic excited states, with 0 the corresponding ground state and r,s intermediate matter states. The transfer is mediated by the virtual photon with wave vector **p**. Panels (a) and (b) illustrate Feynman diagrams for direct RET. (c) One of 24 time orderings representing one type of laser-modified process where both donor and acceptor interact with the auxiliary beam (with wave vector **k**). (d) The mirror case of (c). (e) One of 24 time orderings representative of LARET interactions where only the donor D interacts with the auxiliary beam. (f) Converse case where only A interacts with the auxiliary beam. In each case (c)–(f), photons are absorbed from and emitted back into the laser beam. Cases (c) and (d) require both donor and acceptor to be sited within the beam: in principle, in (e) or (f), only one of them need be.

over three intermediate states R, S, and T:

$$M^{(4)} = \sum_{R,S,T} \frac{\langle F|H_{\rm int}|T\rangle\langle T|H_{\rm int}|S\rangle\langle S|H_{\rm int}|R\rangle\langle R|H_{\rm int}|I\rangle}{(E_I - E_R)(E_I - E_S)(E_I - E_T)}. \quad (8)$$

For this case, by using the notation of Eq. (2), the initial ($|\Psi_I\rangle$) and final ($|\Psi_F\rangle$) matter-radiation states can be expressed as below:

$$|\Psi_I\rangle = |D^\alpha, A^0; n(\mathbf{k}), 0(\mathbf{p})\rangle, \quad (9)$$

$$|\Psi_F\rangle = |D^0, A^\beta; n(\mathbf{k}), 0(\mathbf{p})\rangle. \quad (10)$$

Here, superscripts denote donor and acceptor states α,β, and n is the number of photons in laser field. Further, the throughput radiation (with wave vector **k** and polarization λ) emerges in the final state that is unchanged from its initial state, while the matter system experiences a transfer of energy from D to A. **p** is the corresponding virtual photon wave vector. The virtual photon can be understood as "borrowing" energy from the vacuum. This is entirely consistent with the time-energy uncertainty principle. When the whole system enters its final state, i.e., after the virtual photon is annihilated, energy conservation is restored [35].

Finally, the energy-transfer process modified by the laser field impinging on a donor-acceptor system can be deduced using Fermi's golden rule [36]:

$$\Gamma^{\rm tot}_{\rm laser} = \frac{2\pi}{\hbar}\left|\sum_{m=1}^{\infty} M^{(2m)}\right|^2 \rho, \quad (11)$$

where ρ is the density of final molecular states of the acceptor particle. The even constraint on the value of m is a result of the nature of LARET. This is because in order for the auxiliary laser field to remain unperturbed overall, each matter-field photonic annihilation needs to be coupled with a creation and vice versa [34]. Here, only the second and fourth orders of the perturbation are sufficient as the series rapidly converges for $m \geqslant 3$.

III. OPTICAL CONTROL OF RESONANCE ENERGY TRANSFER

We explore the effects on the process of energy transfer due directly to a laser beam impinging on a donor-acceptor nanostructure system consisting of nanowires and quantum dots. We shall concentrate exclusively on the dominant near-field regime, where the compelling photophysical mechanism, RET, gains control.

A. Nanowire system

Nanowires (NWs) are a specific type of nanostructures with large aspect ratios and small diameters; they have been the

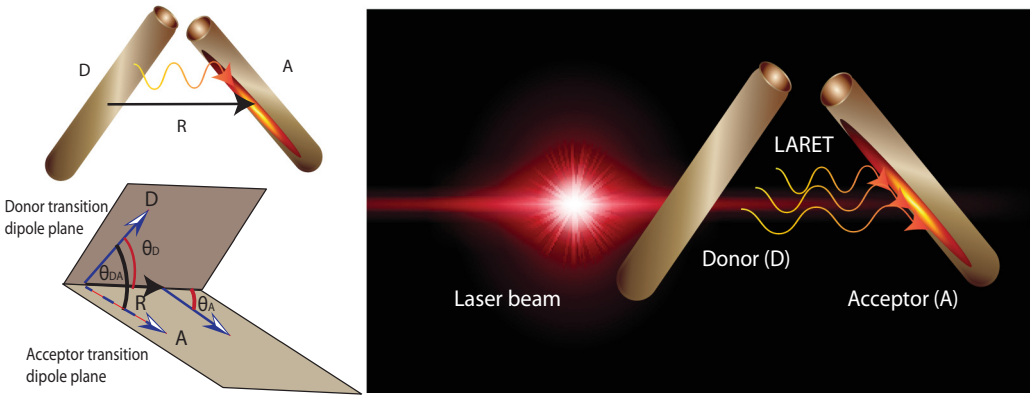

FIG. 3. Schematics for the (a) direct resonance energy transfer in NW to NW with the orientational factors in Eq. (15) (R is the distance between two NWs), and (b) laser-assisted resonance energy transfer (LARET) in a NW pair.

focus of extensive research during the last few decades [37,38]. Their length is commonly sufficiently large for relatively easy manipulation as building blocks in fabricating superstructures. Here, we consider the process of resonance energy transfer in a system consisting of NWs illuminated by an auxiliary laser field as illustrated in Fig. 3(b). Owing to the cylindrical symmetry of NWs, it is convenient to model EM waves using a Hankel function of order n [39–41]. Directly substituting into Eq. (6) yields

$$M_{\mathrm{NW}}^{(2)} = \frac{\mu_i^{0\alpha}(D)\mu_j^{\beta 0}(A)}{8\pi^2 L\epsilon_0}(-\nabla^2\delta_{ij} + \nabla_i\nabla_j) \times \int_0^{\infty}\int_0^{2\pi} \frac{H_0^{(1)}(pR)}{q-p} - \frac{H_0^{(2)}(pR)}{q+p} d\phi dp. \quad (12)$$

The subscripts i and j denote Cartesian components referring to the spatial dimensions, and $\nabla_a \equiv \partial/\partial R_a$. Equation (12) is evaluated by performing contour integration and by necessary vector differentiation to give [26,31]

$$\begin{aligned} M_{\mathrm{NW}}^{(2)} = \frac{\mu_i^{0\alpha}(D)\mu_j^{\beta 0}(A)}{4L\epsilon_0}\Bigg[& q\delta_{ij}\left\{-Y_2(qR) + \frac{Y_1(qR)}{qR}\right\} \\ & - q\left\{Y_1(qR)\left(\frac{\delta_{ij}-\hat{R}_i\hat{R}_j}{R}\right) + q\hat{R}_i\hat{R}_j \right. \\ & \left. \times\left(-Y_2(qR) + \frac{Y_1(qR)}{qR}\right)\right\} - iq\delta_{ij}\left\{-J_2(qR) \right. \\ & \left. + \frac{J_1(qR)}{qR}\right\} + iq\left\{J_1(qR)\left(\frac{\delta_{ij}-\hat{R}_i\hat{R}_j}{R}\right) \right. \\ & \left. + q\hat{R}_i\hat{R}_j\left(-J_2(qR) + \frac{J_1(qR)}{qR}\right)\right\}\Bigg], \end{aligned} \quad (13)$$

where $Y_z(qR)$, $J_z(qR)$ are the second and first kind of Bessel functions, respectively; z is the order number.

Deploying the asymptotic series using standard Gamma function [42] and applying short-range limits $qR \ll 1$ on Eq. (13) yields

$$\begin{aligned} M_{\mathrm{NW}}^{(2)} &= \frac{\mu_i^{0\alpha}(D)\mu_j^{\beta 0}(A)}{2\pi L\epsilon_0 R^2}(\delta_{ij} - 2\hat{R}_i\hat{R}_j) \\ &= \frac{\kappa_{\mathrm{NW}}\left|\mu_i^{0\alpha}(D)\right|\left|\mu_j^{\beta 0}(A)\right|}{2\pi L\epsilon_0 R^2}. \end{aligned} \quad (14)$$

The above equation is dominant in the short-range region and indicates a highly "virtual" character of the electromagnetic mediator. Here, $|\kappa_{\mathrm{NW}}|^2$ is an orientation factor, which describes the influence of the relative orientations of the transition dipole moments of the donor and acceptor NWs, as given by

$$\begin{aligned} \kappa_{\mathrm{NW}} &= \hat{\mu}_i^{0\alpha}(D)(\delta_{ij} - 2\hat{R}_i\hat{R}_j)\hat{\mu}_j^{\beta 0}(A) \\ &= \cos(\theta_{DA}) - 2\cos(\theta_D)\cos(\theta_A), \end{aligned} \quad (15)$$

where θ_D is the angle between donor and interparticle separation vector ($\boldsymbol{R} = R\hat{R}$), and θ_A is the angle between acceptor and $\boldsymbol{R}$. θ_{DA} is the angle between donor and acceptor NWs [see Fig. 3(a)]. Due to the cylindrical symmetry and the physical nature of the exchanged photon in the 2D geometry, the orientation factor varies from $0 \leqslant \kappa_{\mathrm{NW}}^2 \leqslant 1$ [31].

In a similar manner, the quantum amplitude or the resonant dipole-dipole interaction (RDDI) arising from the input auxiliary beam is given by

$$\begin{aligned} M_{\mathrm{NW}}^{(4)} = -\frac{n\hbar ck}{2\epsilon_0 V}\Bigg\{ & e_i^{\lambda}(\boldsymbol{k})\alpha_{ij}^{0\alpha(D)}(k)\frac{(\delta_{jk} - 2\hat{R}_j\hat{R}_k)}{2\pi L\epsilon_0 R^2} \\ & \times \alpha_{kl}^{\beta 0(A)}(k)\bar{e}_l^{\lambda}(\boldsymbol{k}) + \bar{e}_i^{\lambda}(\boldsymbol{k})\alpha_{ij}^{0\alpha(D)}(k)\frac{(\delta_{jk} - 2\hat{R}_j\hat{R}_k)}{2\pi L\epsilon_0 R^2} \\ & \times \alpha_{kl}^{\beta 0(A)}(k)e_l^{\lambda}(\boldsymbol{k}) + e_i^{\lambda}(\boldsymbol{k})\bar{e}_j^{\lambda}(\boldsymbol{k})\beta_{ijk}^{0\alpha(D)}(k) \\ & \times \frac{(\delta_{kl} - 2\hat{R}_k\hat{R}_l)}{2\pi L\epsilon_0 R^2} \times \mu_l^{0\beta(A)} + \mu_i^{0\alpha(D)} \\ & \times \frac{(\delta_{ij} - 2\hat{R}_i\hat{R}_j)}{2\pi L\epsilon_0 R^2} \times e_k^{\lambda}(\boldsymbol{k})\bar{e}_l^{\lambda}(\boldsymbol{k})\beta_{jkl}^{0\alpha(D)}(k)\Bigg\}, \end{aligned} \quad (16)$$

where n is the number of photons (proportional to laser intensity) in the quantization volume V, and e and $\hbar ck$ represent the polarization ($\bar{e}$ denoting its complex conjugation) and energy of the input photon, respectively. Further, $\alpha_{ij}^{fi}(k)$ and $\beta_{ijk}^{fi}(k)$

are generalized polarizability and hyperpolarizability tensors defined as [43,44]

$$\alpha_{ij}^{fi}(k) = \sum_{s}\left\{\frac{\mu_i^{fs}\mu_j^{si}}{E_{sf}-\hbar ck}+\frac{\mu_j^{fs}\mu_i^{si}}{E_{si}+\hbar ck}\right\}, \tag{17}$$

$$\begin{aligned}\beta_{ijk}^{fi}(k) = \sum_{s,t}\Bigg\{&\frac{\mu_i^{ft}\mu_j^{ts}\mu_k^{si}}{(E_{si}-\hbar ck)(E_{ti}-\hbar ck)}\\ &+\frac{\mu_i^{ft}\mu_k^{ts}\mu_j^{si}}{(E_{si}-\hbar ck)(E_{ti}-\hbar ck)}+\frac{\mu_j^{ft}\mu_i^{ts}\mu_k^{si}}{(E_{si}-\hbar ck)(E_{ti}-\hbar ck)}\\ &+\frac{\mu_j^{ft}\mu_k^{ts}\mu_i^{si}}{(E_{si}-\hbar ck)(E_{ti}-\hbar ck)}+\frac{\mu_k^{ft}\mu_i^{ts}\mu_j^{si}}{(E_{si}-\hbar ck)(E_{ti}-\hbar ck)}\\ &+\frac{\mu_k^{ft}\mu_j^{ts}\mu_i^{si}}{(E_{si}-\hbar ck)(E_{ti}-\hbar ck)}\Bigg\}.\end{aligned} \tag{18}$$

Equation (16) represents the optically nonlinear influence of the input beam, involving four components: (i) laser photon absorption at D, stimulated emission at A; (ii) the converse; (iii) absorption and emission at D; and (iv) both photon events at A.

According to Fermi's golden rule given in Eq. (11), the matrix elements of the interaction operator between the initial and final states of the field determine the transition probability

$$\begin{aligned}\Gamma_{\rm NW}^{\rm laser} = &\frac{2\pi\rho}{\hbar}\left|M_{\rm NW}^{(2)}\right|^2+\frac{2\pi\rho}{\hbar}\left|M_{\rm NW}^{(4)}\right|^2\\ &+\frac{4\pi\rho}{\hbar}{\rm Re}\left\{M_{\rm NW}^{(2)}\overline{M}_{\rm NW}^{(4)}\right\}.\end{aligned} \tag{19}$$

The first term represents the normal Förster energy transfer rate

$$\Gamma_{\rm NW}^{(2-2)} = \frac{\left|\mu_i^{0\alpha}(D)\right|^2\left|\mu_j^{\beta 0}(A)\right|^2|\kappa_{\rm NW}|^2\rho}{2\pi L^2R^4\epsilon_0{}^2\hbar}. \tag{20}$$

The middle term depends on the laser intensity, and is explicitly given by

$$\begin{aligned}\Gamma_{\rm NW}^{(4-4)} = &\frac{I^2(k)\rho}{8L^2\hbar c^2\pi\epsilon_0^4R^4}\left|e_i^{\lambda}(\boldsymbol{k})\alpha_{ij}^{0\alpha(D)}(k)\right.\\ &\times(\delta_{jk}-2\hat{R}_j\hat{R}_k)\alpha_{kl}^{\beta 0(A)}(k)\bar{e}_l^{\lambda}(\boldsymbol{k})+\bar{e}_i^{\lambda}(\boldsymbol{k})\alpha_{ij}^{0\alpha(D)}(k)\\ &\times(\delta_{jk}-2\hat{R}_j\hat{R}_k)\alpha_{kl}^{\beta 0(A)}(k)e_l^{\lambda}(\boldsymbol{k})+e_i^{\lambda}(\boldsymbol{k})\bar{e}_j^{\lambda}(\boldsymbol{k})\beta_{ijk}^{0\alpha(D)}(k)\\ &\times(\delta_{kl}-2\hat{R}_k\hat{R}_l)\mu_l^{0\beta(A)}+\mu_i^{0\alpha(D)}(\delta_{ij}-2\hat{R}_i\hat{R}_j)\\ &\left.\times\beta_{jkl}^{0\alpha(D)}(k)e_k^{\lambda}(\boldsymbol{k})\bar{e}_l^{\lambda}(\boldsymbol{k})\right|^2.\end{aligned} \tag{21}$$

Here, $I(k)\equiv n\hbar ck(Lt^{-1})/A(L)=n\hbar c^2k/V$ is the auxiliary laser intensity, described as comprising n photons with wave vector $\boldsymbol{k}$. The third term, linear in I, signifies a quantum interference of these two concurrent processes:

$$\begin{aligned}\Gamma_{\rm NW}^{\rm inter} = &-\frac{I(k)|\mu_i^{0\alpha}(D)||\mu_j^{\beta 0}(A)|\kappa_{\rm NW}\rho}{2L^2\hbar c\pi\epsilon_0^3R^4}\\ &\times{\rm Re}\left\{e_i^{\lambda}(\boldsymbol{k})\alpha_{ij}^{0\alpha(D)}(k)(\delta_{jk}-2\hat{R}_j\hat{R}_k)\alpha_{kl}^{\beta 0(A)}(k)\bar{e}_l^{\lambda}(\boldsymbol{k})\right.\\ &\left.+\bar{e}_i^{\lambda}(\boldsymbol{k})\alpha_{ij}^{0\alpha(D)}(k)(\delta_{jk}-2\hat{R}_j\hat{R}_k)\alpha_{kl}^{\beta 0(A)}(k)e_l^{\lambda}(\boldsymbol{k})\right.\\ &\left.+e_i^{\lambda}(\boldsymbol{k})\bar{e}_j^{\lambda}(\boldsymbol{k})\beta_{ijk}^{0\alpha(D)}(k)(\delta_{kl}-2\hat{R}_k\hat{R}_l)\mu_l^{0\beta(A)}\right.\\ &\left.+\mu_i^{0\alpha(D)}(\delta_{ij}-2\hat{R}_i\hat{R}_j)\beta_{jkl}^{0\alpha(D)}(k)e_k^{\lambda}(\boldsymbol{k})\bar{e}_l^{\lambda}(\boldsymbol{k})\right\}.\end{aligned} \tag{22}$$

By implementing conservative estimates for parameters, $\mu^{0\alpha}(D)\approx\mu^{\beta 0}(A)\approx 5\times10^{-30}$ C m for transition dipole moment magnitudes and $\alpha(D)\alpha(A)\approx\beta(D)\mu(A)\approx\mu(D)\beta(A)\approx 1\times10^{-78}$ C^4 m^2 J^{-2} for tensor products, we can estimate the relative magnitude of the effect with increasing laser intensity. We use the above parameters for the development of the plots in Secs. III A and III B.

Laser irradiance and orientational dependence on transfer rate

We envisage three vital orientational factors and the laser irradiance dependence on each case to enhance the transfer rate.

(1) $\kappa_{\rm NW}=1$. When $\cos(\theta_{DA})=\pi$, $\cos(\theta_D)=\pi$ (or 0), and $\cos(\theta_A)=0$ (or π), the orientation factor $\kappa_{\rm NW}$ becomes 1. Figure 5(a) illustrates the total energy transfer rate and the magnitudes of the individual contributions to the transfer rate with increasing laser intensity. The direct RET rate is constant with respect to I as nonmediated RET is independent of the radiation intensity. The LARET gradually increases with I, showing the quadratic nature of $\Gamma_{\rm NW}^{4-4}$. Nevertheless, quantum interference ($\Gamma_{\rm NW}^{\rm inter}$) linearly decreases with I, owing to the quantum amplitudes of direct and laser-mediated RET [see Fig. 4(a) and Eq. (22)]. These results exhibit a gradual decline of the total energy transfer efficiency until it reaches its minimum point when I becomes 1.33×10^{17} W m^{-2}. After this point, the total energy transfer rate steadily elevates its value and finally starts dominating the direct transfer rate when $I\geqslant 2.66\times10^{17}$ W m^{-2} [see point X in Fig. 5(a)].

(2) $\kappa_{\rm NW}=0$. This is when both transition dipole moments are perpendicular to each other and perpendicular to the donor-acceptor separation vector. This configuration prohibits the direct transfer of energy; hence it excludes the quantum interference. Therefore, only the laser-driven RET term survives, exhibiting a steady increment of total energy transfer rate with respect to I. Transfer rates and corresponding quantum amplitudes are depicted in Figs. 5(b) and 4(b), respectively.

(3) $\kappa_{\rm NW}=-1$. When $\cos(\theta_{DA})=\cos(\theta_D)=\cos(\theta_A)=0$, the orientation factor $\kappa_{\rm NW}$ becomes -1. In this case, the coupling matrix element of direct RET acquires a negative value as illustrated in Fig. 4(c), delivering a positive quantum interference. Analogous to the case of $\kappa_{\rm NW}=1$, laser-mediated RET gradually increases as a function of I and direct RET is independent of I. Thus, the total rate enhances steadily with increasing I, displaying a higher total transfer rate compared to the Förster-type direct RET for the whole spectrum of laser intensities. These results are illustrated in Fig. 5(c).

B. Quantum dot system

In contrast to molecular fluorophores, individual quantum dots (QDs) have discrete atomlike energy transitions, which arise from band splitting due to the quantum confinement effect. Furthermore, QDs exhibit excellent photophysical properties that are highly desirable in a RET system, including

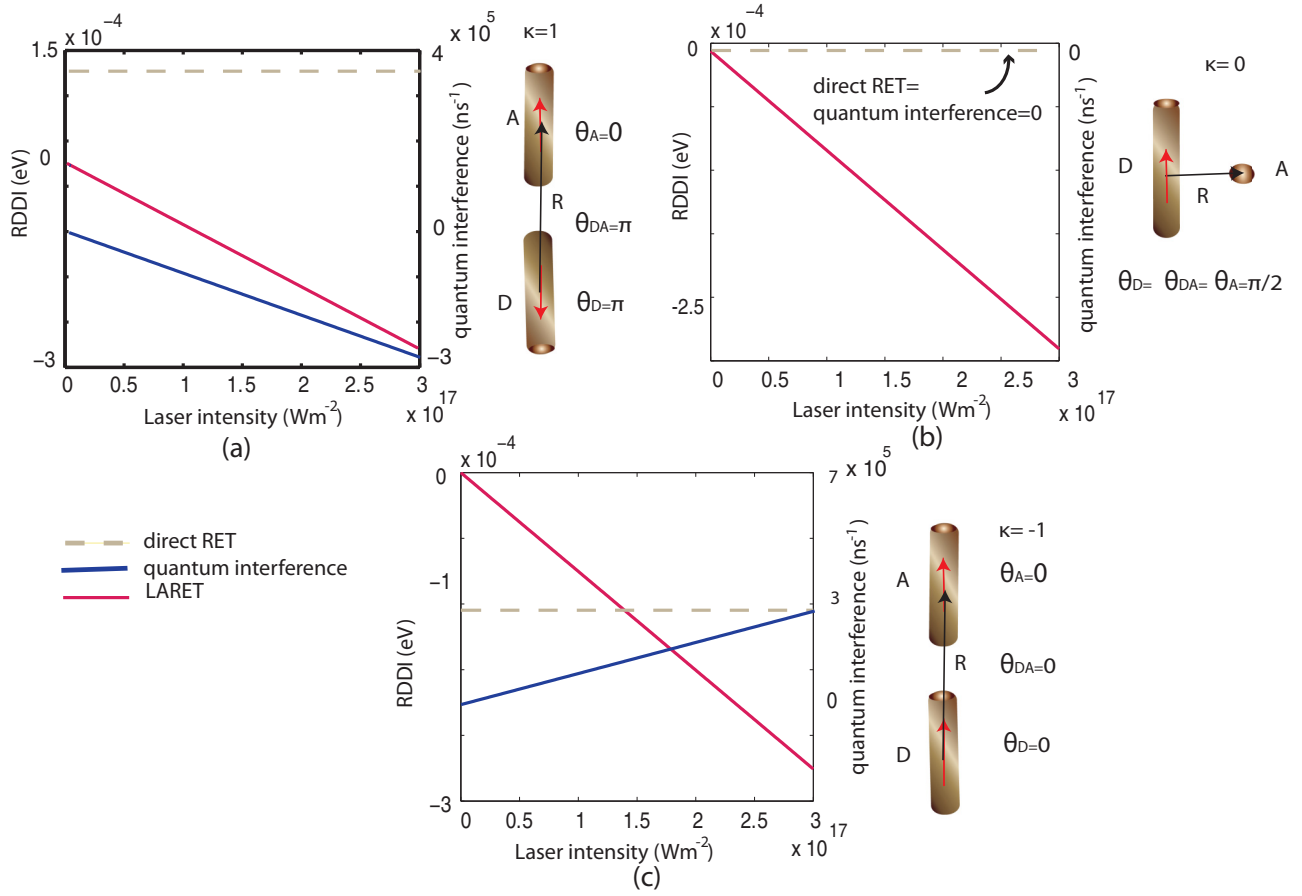

FIG. 4. RDDI strengths of the direct RET (ash colored dashed line), laser-driven RET (pink colored line), and the quantum interference (blue colored line) when $\kappa = 1,0,-1$ are shown in (a)–(c), respectively, as a function of the laser intensity.

(1) broad absorption spectra, (2) large absorption cross sections, and (3) narrow, size-tunable emission spectra, to name a few [45–47]. In this section, a pair of QDs separated by distance R interacting with a laser field is considered as represented in Fig. 6(b). The direct interaction between the donor and acceptor can be calculated from the second-order

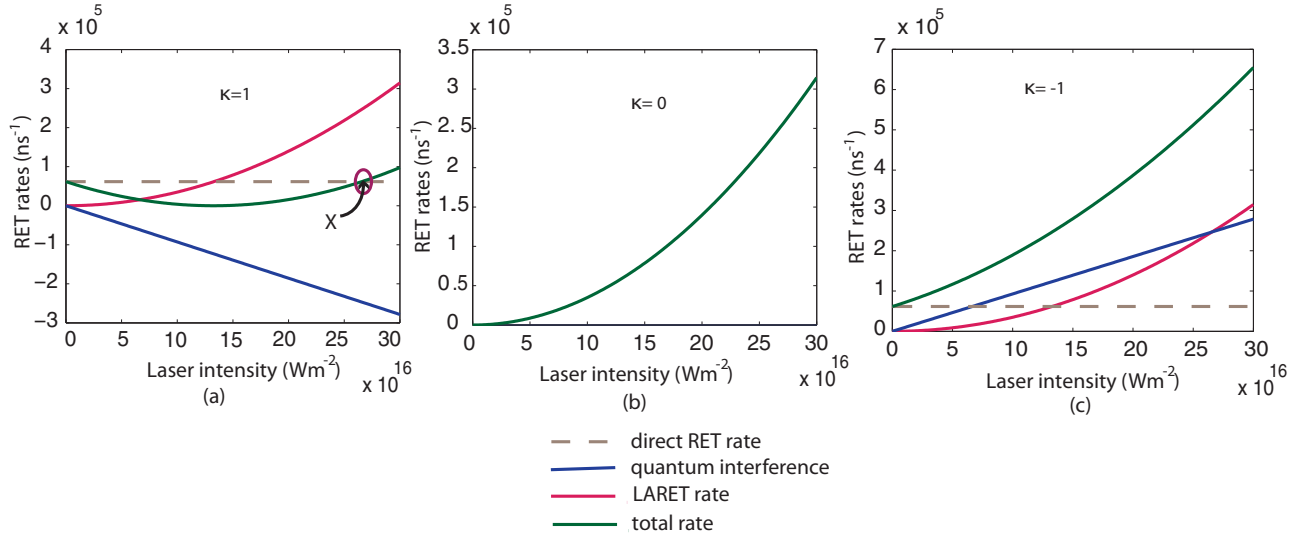

FIG. 5. Transfer rates for energy transfer between nanowires: direct RET (ash colored dashed line), laser-driven RET (red colored line), quantum interference (blue colored line), and the total LARET rate (green colored line) when $\kappa = 1,0,-1$ are shown in (a)–(c), respectively, as a function of the laser intensity.

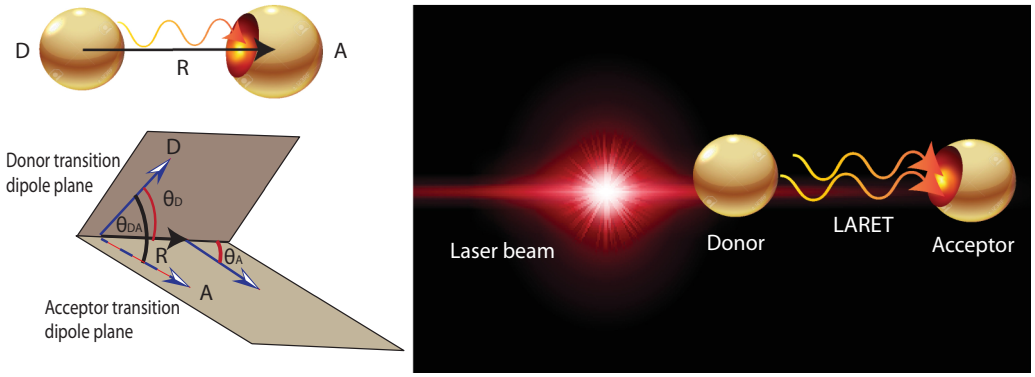

(a) (b)

FIG. 6. Schematics for the (a) direct resonance energy transfer in QD to QD with the orientational factors in Eq. (26) (R is the distance between two QDs), and (b) laser-assisted resonance energy transfer (LARET) in a QD pair.

quantum amplitude [30,48]:

$$M_{\rm QD}^{(2)} = \frac{\mu_i^{0\alpha}(D)\mu_j^{\beta 0}(A)}{16\pi^3\epsilon_0}(-\nabla^2\delta_{ij} + \nabla_i\nabla_j)\int_0^\infty\int_0^{2\pi}\int_{-1}^{1} \times\left\{\frac{e^{i\boldsymbol{p}\cdot\boldsymbol{R}}p}{q-p} - \frac{e^{-i\boldsymbol{p}\cdot\boldsymbol{R}}p}{q+p}\right\}d(\cos\theta)d\phi dp. \quad (23)$$

Performing contour integration with a suitable contour by the residue theorem and applying near-field limits yields

$$M_{\rm QD}^{(2)} = \mu_i^{0\alpha}(D)\frac{\delta_{ij} - 3\hat{R}_i\hat{R}_j}{4\pi\epsilon_0 R^3}\mu_j^{\beta 0}(A). \quad (24)$$

The application of Fermi's golden rule gives rise to the following expression for the direct energy transfer rate between two QDs:

$$\Gamma_{\rm QD}^{(2-2)} = \frac{\left|\mu_i^{0\alpha}(D)\right|^2\left|\mu_j^{\beta 0}(A)\right|^2|\kappa_{\rm QD}|^2\rho}{8\pi R^6\epsilon_0{}^2\hbar}, \quad (25)$$

where $|\kappa_{\rm QD}|^2$ is an orientation factor,

$$\kappa_{\rm QD} = \hat{\mu}_i^{0\alpha}(D)(\delta_{ij} - 3\hat{R}_i\hat{R}_j)\hat{\mu}_j^{\beta 0}(A) = \cos(\theta_{DA}) - 3\cos(\theta_D)\cos(\theta_A). \quad (26)$$

Here, θ_D is the angle between donor and separation vector ($\boldsymbol{R}$), and θ_A is the angle between acceptor and $\boldsymbol{R}$. θ_{DA} is the angle between donor and acceptor QDs [Fig. 6(a)]. Owing to the spherical symmetry of the QDs, the orientation factor varies from $0 \leqslant \kappa_{\rm QD}^2 \leqslant 4$.

The indirect transfer rate $\Gamma_{\rm QD}^{(4-4)}$ represents the optically nonlinear influence of the input beam and is delivered by previous work [34,49],

$$\Gamma_{\rm QD}^{(4-4)} = \frac{I^2(k)\rho}{32\hbar c^2\pi\epsilon_0^4 R^6}\left|e_i^\lambda(\boldsymbol{k})\alpha_{ij}^{0\alpha(D)}(k) \times(\delta_{jk} - 3\hat{R}_j\hat{R}_k)\alpha_{kl}^{\beta 0(A)}(k)\bar{e}_l^\lambda(\boldsymbol{k}) + \bar{e}_i^\lambda(\boldsymbol{k})\alpha_{ij}^{0\alpha(D)}(k) \times(\delta_{jk} - 3\hat{R}_j\hat{R}_k)\alpha_{kl}^{\beta 0(A)}(k)e_l^\lambda(\boldsymbol{k}) + e_i^\lambda(\boldsymbol{k})\bar{e}_j^\lambda(\boldsymbol{k})\beta_{ijk}^{0\alpha(D)}(k) \times(\delta_{kl} - 3\hat{R}_k\hat{R}_l)\mu_l^{0\beta(A)} + \mu_i^{0\alpha(D)}(\delta_{ij} - 3\hat{R}_i\hat{R}_j) \times\beta_{jkl}^{0\alpha(D)}(k)e_k^\lambda(\boldsymbol{k})\bar{e}_l^\lambda(\boldsymbol{k})\right|^2. \quad (27)$$

Thus, the quantum interference due to the laser field is given by

$$\Gamma_{\rm QD}^{\rm inter} = -\frac{I(k)|\mu_i^{0\alpha}(D)||\mu_j^{\beta 0}(A)|\kappa_{\rm QD}\rho}{8\hbar c\pi\epsilon_0^3 R^6} \times Re\left\{e_i^\lambda(\boldsymbol{k})\alpha_{ij}^{0\alpha(D)}(k)(\delta_{jk} - 3\hat{R}_j\hat{R}_k)\alpha_{kl}^{\beta 0(A)}(k)\bar{e}_l^\lambda(\boldsymbol{k}) + \bar{e}_i^\lambda(\boldsymbol{k})\alpha_{ij}^{0\alpha(D)}(k)(\delta_{jk} - 3\hat{R}_j\hat{R}_k)\alpha_{kl}^{\beta 0(A)}(k)e_l^\lambda(\boldsymbol{k}) + e_i^\lambda(\boldsymbol{k})\bar{e}_j^\lambda(\boldsymbol{k})\beta_{ijk}^{0\alpha(D)}(k)(\delta_{kl} - 3\hat{R}_k\hat{R}_l)\mu_l^{0\beta(A)} + \mu_i^{0\alpha(D)}(\delta_{ij} - 3\hat{R}_i\hat{R}_j)\beta_{jkl}^{0\alpha(D)}(k)e_k^\lambda(\boldsymbol{k})\bar{e}_l^\lambda(\boldsymbol{k})\right\}. \quad (28)$$

Laser irradiance and orientational dependence on RET rate

Proceeding as with NW systems, we study three nontrivial orientational factors and the laser irradiance dependence on each case to enhance the transfer rate.

(1) $\kappa_{\rm QD} = 2$. Similarly to the NW case, the laser-modified coupling matrix element ($M_{\rm QD}^{(4-4)}$) decreases with intensity while direct coupling remains static for all the laser intensities, producing a negative quantum interference value which steadily declines as a function of I. This is shown in Fig. 7(a). As depicted in Fig. 8(a), the LARET in QDs gradually increases with I. On the other hand quantum interference leads to a steady drop when I increases, displaying a gradual decline in the total energy transfer rate until I reaches its value of 2.66×10^{17} W m^{-2}. It is immediately apparent that at intensities less than 2.66×10^{17} W m^{-2}, the transfer is Förster dominated. Due to the effect of LARET, total energy transfer elevates with increasing I and finally achieves higher transfer efficiencies when $I \geqslant 5.32\times10^{17}$ W m^{-2} [see point Y in Fig. 8(a)].

(2) $\kappa_{\rm QD} = 0$. This case is analogous to the case of $\kappa_{\rm NW} = 0$. Here the direct coupling has been "switched off" between QD particles by arranging them such that the transition dipole moments are perpendicular to each other and the donor-acceptor separation vector, hence excluding the quantum interference. Therefore, the total energy transfer only contains the contribution of laser-dependent RET, which gradually increases as a function of I. These results are shown in Fig. 7(b) and Fig. 8(b).

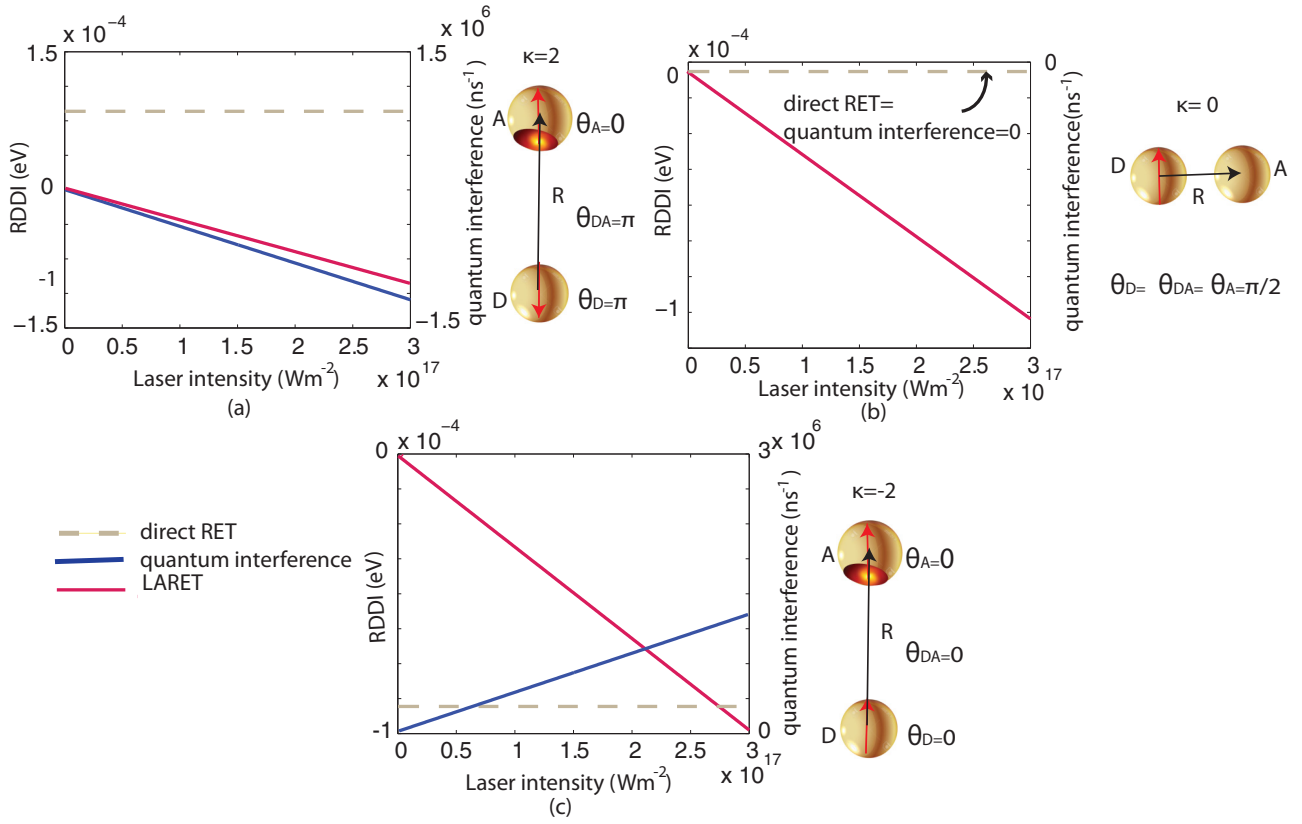

FIG. 7. RDDI strengths of the direct RET (ash colored dashed line), laser-driven RET (pink colored line), and the quantum interference (blue colored line) when $\kappa = 2, 0, -2$ are shown in (a)–(c), respectively, as a function of the laser intensity.

(3) $\kappa_{QD} = -2$. This is when both transition dipole moments are parallel to each other and parallel to the donor-acceptor separation vector. The quantum amplitude of direct RET acquires a negative value as depicted in Fig. 7(c), resulting in a positive quantum interference. Analogous to the case of $\kappa_{QD} = 2$, laser-mediated RET gradually increases as a function of I and direct RET is independent of I. Therefore, the total rate enhances steadily with increasing I. Here, the direct RET between a pair

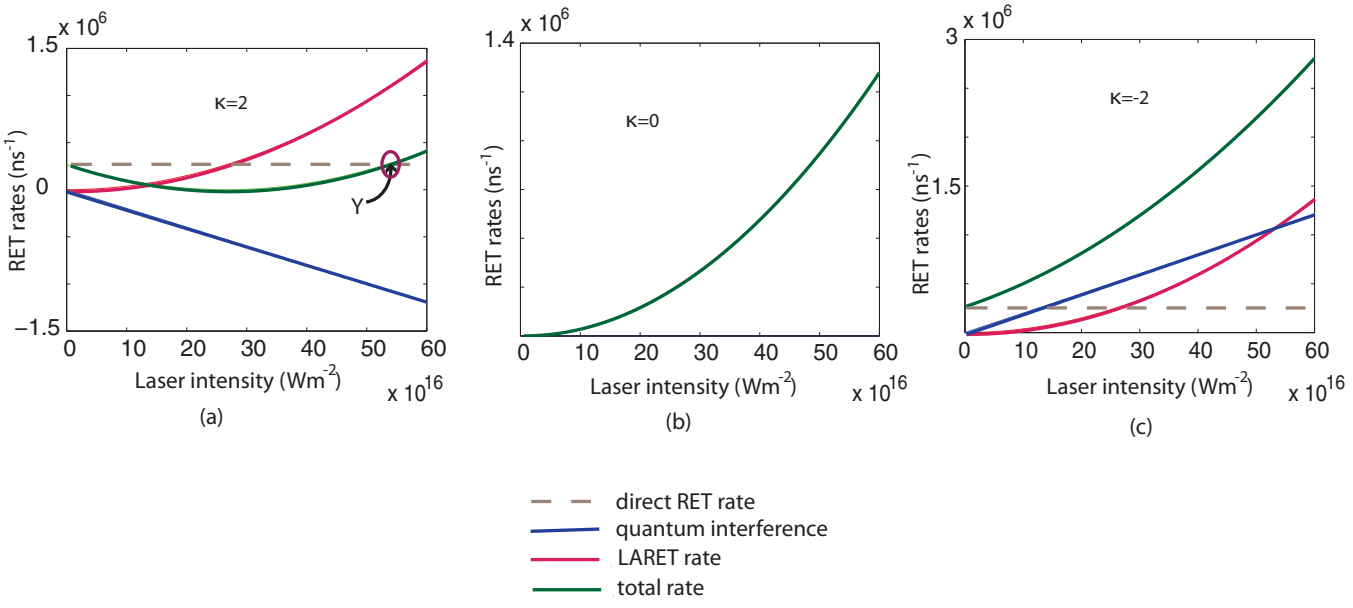

FIG. 8. Transfer rates for energy transfer between quantum dots: direct RET (ash colored dashed line), laser-driven RET (red colored line), quantum interference (blue colored line), and the total LARET rate (green colored line) when $\kappa = 2, 0, -2$ are shown in (a)–(c), respectively, as a function of the laser intensity.

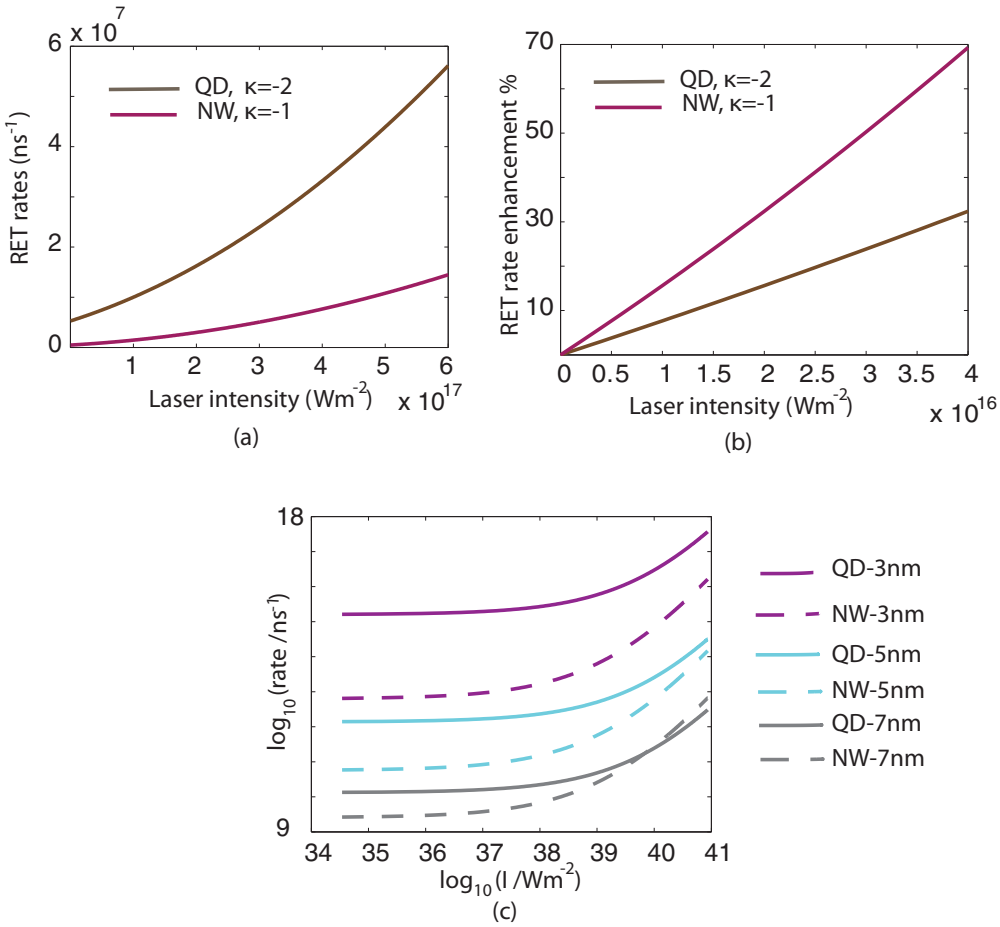

FIG. 9. (a) The brown and purple solid lines represent the LARET rates; (b) RET rate enhancement factor in QD and NW systems; (c) log-log plot of transfer rate as a function of $\log(I)$, for three different relative distances (3 nm, 5 nm, 7 nm) between D and A, dashed lines representing the transfer rates for the case of a NW pair. Note that for all the plots from (a)–(c), we consider $\kappa_{\mathrm{NW}} = -1$ and $\kappa_{\mathrm{QD}} = -2$.

of QDs is dominated by the LARET for the whole spectrum of laser intensities. These results are shown in Fig. 8(c).

C. Design guidelines for high-efficiency laser-driven RET

The RET rate can be enhanced efficiently, when the optimal configuration of the nanostructure system is implemented. Here, the fastest transfer between nearby sites occurs where the particle transition dipole moments and the separation vector are collinear ($\theta_{DA} = \theta_D = \theta_A = 0$). The transfer rate enhancement with increasing laser intensity for this scenario is depicted in Fig. 9(a), comparing both QD and NW cases. The results of further calculations to exhibit RET rate enhancement as a percentage [Fig. 9(b)] demonstrate that even for moderate laser intensities ($I \approx 4\times10^{16}$ W m^{-2}), up to 32% and 70% rate enhancements can be achieved for QDs and NWs, respectively.

Furthermore, we investigated the distance dependence in laser-driven RET in NWs and QDs. Owing to the $(R)^{-4}$ and $(R)^{-6}$ distance dependence on the total transfer rate in NW and QD respectively, lower relative spacing between donor and acceptor particles displays higher transfer efficiency. This is shown in Fig. 9(c). Moreover, it can also be observed from the plots that QDs produce higher LARET efficiency in relatively lower intensities. However, when increasing the laser beam intensity, LARET in NWs qualitatively starts to outperform QDs.

IV. DISCUSSION

In Sec. III, laser-driven resonance energy transfer rate equations and corresponding quantum amplitudes and quantum interferences for nanowire and quantum dot systems have been derived and the results exhibited graphically. The results have demonstrated that the transfer of energy can be enhanced to a significant and measurable degree when the laser intensity is pulsed and highly focused, or through deploying favorable configurations of the nanostructure particles ($\kappa_{\mathrm{NW}} = -1, \kappa_{\mathrm{QD}} = -2$). It is also important that the laser radiation is off-resonant, in order to prevent direct excitation of the acceptor.

Exploration of the quantum amplitudes in laser-assisted RET is the core contribution of all derivations. Our calculations for quantum amplitude are based on the Schrödinger state vector representation of quantum dynamics, where the matrix element for RET is represented as a sum of differently time-ordered contributions [26]. Figures 4(a)–4(c) indicate the variation of RDDI strengths in a NW pair against the laser irradiance for different orientation factors. Interestingly, laser-driven RDDIs are identical for all three cases. This is because the quantum amplitude for laser-driven RET is independent of the orientational factor. Nevertheless, direct RET and quantum interference contributions to the transfer

rate vary with κ, and vanish when NWs are perpendicular to each other and to the distance vector. The variations of RDDIs of QDs with laser irradiation and orientational factor exhibit similar patterns observed for NWs [Figs. 7(a)–7(c)], with one difference. Due to the physical nature and geometry of the quantum dots, the κ_{QD} value is higher than the κ_{NW}.

Furthermore, rates for unmediated RET, laser-driven RET, and the quantum interference for a pair of NWs are illustrated in Figs. 5(a)–5(c) for three nontrivial orientational factors. In Fig. 5(a), where the Γ^{tot} is plotted against laser irradiation when $\kappa_{\mathrm{NW}} = 1$, a gradual decrement and then an increment of total transfer rate with the laser intensity can be observed. Here, when the laser intensity is low, quantum interference dominates the transfer rate. However, when the intensity increases, laser-assisted RET dominates the transfer process and finally for high intensities, an enhancement in RET rate can be observed. Moreover, when $\kappa_{\mathrm{NW}} = 0$ [Fig. 5(b)], direct RET and hence the quantum interference are explicitly forbidden, allowing full control to the laser-driven transfer. In this case, optical switching can be produced by the throughput of a single off-resonant beam (or, with more control options, by two coincident beams) [49–51]. Further, for angles $\theta_{DA} = \theta_D = \theta_A = 0$, a gradual increase of the total transfer rate against laser intensity can be observed as depicted in Fig. 5(c). Thus the RET rate can be enhanced to a greater extent under this condition. Additionally, the results for QDs show similar patterns [Figs. 8(a)–8(c)] and hold same explanations, with one significant difference. Due to the nature of the real and virtual photon in spherical geometry, when $\kappa_{\mathrm{QD}} = 2$ ($\theta_{DA} = \theta_D = \pi, \theta_A = 0$), higher laser intensities are needed to suppress the quantum interference which arises from the applied laser beam.

V. CONCLUSIONS AND OUTLOOK

We calculated the rates of laser-driven resonance energy transfer in optically excited systems composed of NWs and QDs. A full quantum electrodynamical treatment for laser-assisted energy migration has been developed and formulated with the aid of Feynman diagram methods [52]. In a nutshell, the results expounded here indicate that at relatively higher laser intensities, the higher-order effects are significant even in a nonfavorable configuration of the particles (when donor-acceptor particles make an angle of π with each other and one particle is parallel to the donor-acceptor displacement vector). Besides, the results show that, at reasonable levels of laser intensity, quantum interference arising from the auxiliary laser beam drops to insignificant levels, enhancing the total RET rate between nanostructures. Thus, at suitable laser intensities, for example those readily available from a focused, mode-locked laser or a spaser, the energy-transfer rate is explicitly enhanced up to 70%.

Moreover, by suitably configuring an arrangement of transition dipoles, it proves possible to design optical switches [53]. Here, the optical switching actions can be implemented by exploiting RET mechanism activated by throughput laser radiation of an appropriate intensity, frequency, and polarization. Spatially correlated donor and acceptor arrays can be assessed as potential realizations for all-optical switching. In this case, the device architecture for such a switch involves thin-film deposits on parallel substrates—an ordered set of nanowires (or quantum dots) being contained within these films. The dipole moments in one film should be arranged perpendicular to the dipole moments in the other layer [49]. Therefore, implemented in a configuration with nanoparticles arrayed in thin films, the process may offer design of logic gates, optical transistor and ultrafast parallel-processing capabilities, etc. This represents scope for potential development of the theory.

In addition to the calculations presented in this article, it is possible to envisage high-intensity nanolasers based on spasers to enhance and control the process of RET. In this case, the emitted photons from and into the laser beam are replaced by surface plasmons. The electric field operator for the surface plasmons would modify the quantum amplitudes and the transfer rate, providing a high-efficiency controlling mechanism for resonance energy transfer.

The ensuing results open up a new avenue for applications of high-efficiency artificial nanoantenna systems. Furthermore, the proposed laser-driven RET mechanism holds potential for optical transistors and optical logic gates, providing building blocks for more complex nanophotonic circuitry.

ACKNOWLEDGMENTS

The work of D.W. is supported by the Monash University Institute of Graduate Research. The work of M.P. is supported by the Australian Research Council, through its Discovery Grant No. DP140100883.

[1] L. Hu and G. Chen, Nano Lett. **7**, 3249 (2007).
[2] G. Rosaz, B. Salem, N. Pauc, P. Gentile, A. Potié, A. Solanki, and T. Baron, Semicond. Sci. Technol. **26**, 085020 (2011).
[3] Y.-L. Lee, B.-M. Huang, and H.-T. Chien, Chem. Mater. **20**, 6903 (2008).
[4] B. A. Kairdolf, A. M. Smith, T. H. Stokes, M. D. Wang, A. N. Young, and S. Nie, Annu. Rev. Anal. Chem. **6**, 143 (2013).
[5] H. Wu, G. Chan, J. W. Choi, Y. Yao, M. T. McDowell, S. W. Lee, A. Jackson, Y. Yang, L. Hu, and Y. Cui, Nat. Nanotechnol. **7**, 310 (2012).
[6] P. Krogstrup, H. I. Jørgensen, M. Heiss, O. Demichel, J. V. Holm, M. Aagesen, J. Nygard, and A. Fontcuberta i Morral, Nat. Photon. **7**, 306 (2013).
[7] C. S. Kumarasinghe, M. Premaratne, S. D. Gunapala, and G. P. Agrawal, Sci. Rep. **6**, 21470 (2016).
[8] D. Sikdar, I. D. Rukhlenko, W. Cheng, and M. Premaratne, Plasmonics **9**, 659 (2014).
[9] M. Premaratne and G. P. Agrawal, *Light Propagation in Gain Media* (Cambridge University Press, Cambridge, 2011).
[10] S. Brichkin, High Energy Chem. **47**, 277 (2013).
[11] P. L. Hernández-Martínez and A. O. Govorov, Phys. Rev. B **78**, 035314 (2008).
[12] V. I. Novoderezhkin, M. A. Palacios, H. Van Amerongen, and R. Van Grondelle, J. Phys. Chem. B **108**, 10363 (2004).
[13] K. Becker, J. M. Lupton, J. Müller, A. L. Rogach, D. V. Talapin, H. Weller, and J. Feldmann, Nat. Mater. **5**, 777 (2006).

[14] V. Raicu, J. Biol. Phys. **33**, 109 (2007).
[15] I. Medintz and N. Hildebrandt, *FRET-Förster Resonance Energy Transfer: From Theory to Applications* (John Wiley & Sons, Weinheim, Germany, 2013).
[16] C. Rupasinghe, I. D. Rukhlenko, and M. Premaratne, ACS Nano **8**, 2431 (2014).
[17] C. Jayasekara, M. Premaratne, M. I. Stockman, and S. D. Gunapala, J. Appl. Phys. **118**, 173101 (2015).
[18] C. Jayasekara, M. Premaratne, S. D. Gunapala, and M. I. Stockman, J. Appl. Phys. **119**, 133101 (2016).
[19] R. J. Cogdell, A. T. Gardiner, A. W. Roszak, C. J. Law, J. Southall, and N. W. Isaacs, Photosynth. Res. **81**, 207 (2004).
[20] M. Mohseni, P. Rebentrost, S. Lloyd, and A. Aspuru-Guzik, J. Chem. Phys. **129**, 174106 (2008).
[21] S. Zhang, Z. Lü, Y. Peng, Y. Liu, and Y. Yang, J. Lumin. **128**, 1523 (2008).
[22] G. D. Scholes, G. R. Fleming, A. Olaya-Castro, and R. van Grondelle, Nat. Chem. **3**, 763 (2011).
[23] T. Förster, Ann. Phys. **437**, 55 (1948).
[24] J. Avery, J. S. Proc. Phys. Soc. **88**, 1 (1966).
[25] L. Gomberoff and E. A. Power, Proc. Phys. Soc. **88**, 281 (1966).
[26] D. P. Craig and T. Thirunamachandran, *Molecular Quantum Electrodynamics* (Dover, New York, 1998).
[27] A. Salam, *Molecular Quantum Electrodynamics: Long-Range Intermolecular Interactions* (Wiley, Hoboken, NJ, 2010).
[28] J. J. Rodriguez and A. Salam, Chem. Phys. Lett. **498**, 67 (2010).
[29] A. Salam, J. Chem. Phys. **136**, 014509 (2012).
[30] D. Weeraddana, M. Premaratne, and D. L. Andrews, Phys. Rev. B **92**, 035128 (2015).
[31] D. Weeraddana, M. Premaratne, and D. L. Andrews, Phys. Rev. B **93**, 075151 (2016).
[32] D. L. Andrews and J. M. Leeder, J. Chem. Phys. **130**, 034504 (2009).
[33] B. Oswald, F. Lehmann, L. Simon, E. Terpetschnig, and O. S. Wolfbeis, Anal. Biochem. **280**, 272 (2000).
[34] P. Allcock, R. D. Jenkins, and D. L. Andrews, Phys. Rev. A **61**, 023812 (2000).
[35] D. L. Andrews and D. S. Bradshaw, Ann. Phys. **526**, 173 (2014).
[36] P. A. M. Dirac, Proc. R. Soc. London A **114**, 243 (1927).
[37] Y. P. Rakovich, F. Jäckel, J. F. Donegan, and A. L. Rogach, J. Mater. Chem. **22**, 20831 (2012).
[38] X. Duan, Y. Huang, Y. Cui, J. Wang, and C. M. Lieber, Nature (London) **409**, 66 (2001).
[39] F. Frezza, L. Pajewski, D. Saccoccioni, and G. Schettini, Opt. Commun. **265**, 47 (2006).
[40] R. Bennett, T. M. Barlow, and A. Beige, Eur. J. Phys. **37**, 014001 (2015).
[41] R. El-Ganainy and S. John, New J. Phys. **15**, 083033 (2013).
[42] M. Abramowitz and I. A. Stegun, *Handbook of Mathematical Functions: With Formulas, Graphs, and Mathematical Tables* (Courier Corporation, New York, 1964).
[43] P. R. Berman, R. W. Boyd, and P. W. Milonni, Phys. Rev. A **74**, 053816 (2006).
[44] P. W. Milonni, R. Loudon, P. R. Berman, and S. M. Barnett, Phys. Rev. A **77**, 043835 (2008).
[45] I. L. Medintz and H. Mattoussi, Phys. Chem. Chem. Phys. **11**, 17 (2009).
[46] U. Resch-Genger, M. Grabolle, S. Cavaliere-Jaricot, R. Nitschke, and T. Nann, Nat. Meth. **5**, 763 (2008).
[47] J. M. Klostranec and W. C. Chan, Adv. Mater. **18**, 1953 (2006).
[48] G. D. Scholes and D. L. Andrews, Phys. Rev. B **72**, 125331 (2005).
[49] D. S. Bradshaw and D. L. Andrews, Superlattices Microstruct. **47**, 308 (2010).
[50] D. S. Bradshaw and D. L. Andrews, J. Chem. Phys. **128**, 144506 (2008).
[51] D. L. Andrews, R. G. Crisp, and S. Li, J. Chem. Phys **127**, 174702 (2007).
[52] R. D. Mattuck, *A Guide to Feynman Diagrams in the Many-Body Problem* (Dover, New York, 1992).
[53] D. S. Bradshaw and D. L. Andrews, J. Nanophoton. **3**, 031503 (2009).